SAMSO-TR-70-44

RADIATION FROM AIR-TEFLON BOUNDARY LAYERS

R.A. Greenberg, K.L. Wray, L.A. Young, et al.

AVCO EVERETT RESEARCH LABORATORY

AMP 294
MARCH 1970

jointly sponsored by
ADVANCED RESEARCH PROJECTS AGENCY
DEPARTMENT OF DEFENSE
ARPA Order #1092
and
SPACE AND MISSILE SYSTEMS ORGANIZATION
AIR FORCE SYSTEMS COMMAND
DEPUTY FOR RE-ENTRY SYSTEMS (SMY)
Norton Air Force Base, California 92409

SAMSO-TR-70-44 AMP 294

RADIATION FROM AIR-TEFLON BOUNDARY LAYERS*†

by

R. A. Greenberg, K. L. Wray, L. A. Young and N. H. Kemp

March 1970

AVCO EVERETT RESEARCH LABORATORY
a division of
AVCO CORPORATION
Everett, Massachusetts

*This research was supported by the Advanced Research Projects Agency of the Department of Defense and Space and Missile Systems Organization, Air Force Systems Command and was monitored by Space and Missile Systems Organization, Air Force Systems Command under Contract F04701-69-C-0036.

†Submitted to AIAA Progress in Astronautics Series

FOREWORD

Distribution of this document is unlimited. This indicates document has been cleared for public release by competent authority.

"This research was supported by the Advanced Research Projects Agency of the Department of Defense and Space and Missile Systems Organization, Air Force Systems Command and was monitored by Space and Missile Systems Organization, Air Force Systems Command under Contract F04701-68-C-0036." The secondary report number as assigned by AERL is Avco Everett Research Laboratory AMP 294. The Air Force program monitor for this contract is Lt. R. W. Padfield, USAF, Project Officer, Environmental Technology Branch, SMYSE.

Publication of this report does not constitute Air Force approval of the report's findings or conclusions; it is published only for the exchange and stimulation of ideas.

Lt. R. W. Padfield, USAF,
Project Officer,
Environmental Technology Branch,
SMYSE

ABSTRACT

Radiation profiles in an ablating flat plate Air-Teflon laminar boundary layer have been studied both experimentally and theoretically. The experiments were conducted in a one atmosphere, 3000 - 6000°K, subsonic free stream produced by an arc jet. Spatially resolved radiation profiles within the boundary layer were obtained in both the visible and near infrared. Spatially integrated boundary layer radiation was measured in the 4 - 10μ region. The major radiation in the visible and near ultraviolet wavelengths was the CN violet. In the infrared, the major radiators were CO, CO_2, NO and COF_2. The theory which was developed to predict the structure included coupling of the heat and mass transfer at the Teflon surface. A "partial equilibrium" model for the Teflon-air chemistry was utilized, which does not allow the formation of CF_3 and CF_4 within the boundary layer. For the selected wavelengths in the infrared the theory generally predicted quite well both the spatial location and magnitude of the peak radiation, and also predicted the integrated radiation across the layer to within a factor of two. For the selected wavelength in the visible, the radiation intensity, which comes from CN, is much larger than predicted, indicating that the CN is not in thermodynamic equilibrium.

TABLE OF CONTENTS

LIST OF SYMBOLS

a, b	constants, Eq. (12)
C	total mass fraction
$\overline{C}$	nucleus mass fraction in gas
f	stream function, Eq. (4)
g	dimensionless enthalpy
h	static enthalpy
H	stagnation enthalpy
I	radiation intensity
q	heat transfer rate
T	temperature
u	x component of velocity
v	y component of velocity
x	distance along surface
y	distance normal to surface
η	Howarth-Dorodnitsyn similarity variable, Eq. (3)
μ	viscosity
ξ	Howarth-Dorodnitsyn streamwise variable, Eq. (3)
ρ	density

Subscripts

A	ablation products
e	free stream conditions
i	nucleus

r	reference condition
so	solid cold Teflon
w	wall
o	leading edge conditions

I. INTRODUCTION

Ablating materials are used extensively to protect hypersonic vehicles from the effects of aerodynamic heating. The theories which have been developed to predict the overall ablation rate of these materials are generally in good agreement with measurements; however, very few measurements have been made of the detailed structure of ablating boundary layers. Measurements of velocity or enthalpy are difficult because of the small dimensions of ablating boundary layers in available high temperature facilities, and the extremely high temperatures involved. More important, ablating materials generally react chemically with the high temperature air, forming new compounds, and altering the temperature profiles; at present there are no direct measurements of the chemical composition or the chemical processes. However, radiation is emitted from the high temperature species in the boundary layer. This radiation is of interest since it can be used as a diagnostic tool to yield information on the chemical composition and processes which take place within the boundary layer. The work described here is an experimental and theoretical study of an ablating air-Teflon boundary layer, using spatially resolved radiation at selected wavelengths as the principal diagnostic tool. The purpose of this study is to increase our understanding of the mechanism by which ablation products react with hot air, both within the boundary and at the ablating surface. Teflon has a particular advantage in this study since it ablates uniformly, leaving no char or liquid layers, and its chemical reactions with air are less complex than hydrocarbon ablators.

The ablating boundary layer was obtained experimentally by passing a subsonic stream of hot air from an arc jet over a Teflon sample placed parallel to the stream. The equilibrium temperature of the air was varied from 3000 to 6000°K at one atmosphere pressure. The resulting boundary layer has a hot, subsonic outer edge and a steadily decreasing enthalpy toward the cooler wall. A quantitative discussion of the utility of the present arc jet experiments is given in Ref. 1.

A unique feature of most of the experiments presented here is the high degree of spatial resolution attained within the boundary layer, which is about 3 mm thick. In the visible region, calibrated spectral plates were used to obtain a resolution of about one-tenth of the boundary layer thickness. The near infrared (1 - 5.5μ) data was obtained with a scanning slit coupled to an IR monochromator, which permitted spatial resolution of about one-sixth the boundary layer thickness. Beyond 5.5μ experimental difficulties prohibited continuation of the spatially resolved measurements; only integrated radiation measurements were obtained.

This paper is a summary of previous work on Teflon ablation contained in Refs. 2, 3 and 4. The visible data was originally presented in Ref. 2, where the principal radiator was found to be CN. The near infrared data of Ref. 3 was attributed to CO, CO_2, NO and possibly COF_2. The 8μ data of Ref. 4 confirmed the presence of COF_2 in the boundary layer. The theoretical model for the ablation process discussed here was discussed previously in Ref. 3. The combined results of Refs. 3 and 4 greatly extend out understanding of Teflon ablation under the experimental conditions.

The prediction of radiation profiles provides a very stringent test of a boundary layer theory and its chemical reaction model since the

calculation of the radiation from a point in the boundary layer requires accurate knowledge of the gas composition, temperature, and radiation intensity per particle; however, the concentrations of the radiating species vary by orders of magnitude across the layer, while the radiation intensity per particle is usually strongly temperature dependent. For example, as will be shown later, the visible radiation in a high temperature ($\sim 6000^{\circ}K$) air-Teflon boundary layer is primarily due to CN radiation even though CN is present only as a trace species in the boundary layer.

The theory which was developed is the simplest which could be devised that contains the relevant chemistry. The laminar boundary layer equations are coupled to the Teflon surface through heat and mass balances, using a constant ablation temperature for Teflon. Chemical nonequilibrium effects are taken into account by a "partial-equilibrium" chemistry model, which does not allow the formation of CF_3 and CF_4. The presence of a cooled boundary layer on the nozzle upstream of the Teflon plate is accounted for by use of a nonsimilar computational procedure.

A detailed discussion of the methods which were used to obtain the radiation measurements is presented in Section II. Section III presents the nonsimilar boundary layer theory which was used to predict the characteristics of the ablating boundary layer, while Section IV contains a comparison of theory and experiment. Finally some concluding remarks are presented in Section V.

BLANK PAGE

II. EXPERIMENTAL METHODS

The arc facility used in the experiments has been described in some detail in Refs. 1 and 2. The arc generates air at temperatures between 3000 to 6000°K at a pressure of one atmosphere, using about 300 kW of input power from a battery bank. Exit plane flow velocities are about 10^5 cm/sec. A schematic diagram of the arc is shown in Fig. 1.

Nitrogen is introduced tangentially at (A) adjacent to the tungsten-tipped cathode. This results in a swirling flow around the cathode as the gas moves into the anode section (B), thus stabilizing the arc by constricting it to the anode centerline. Oxygen is introduced downstream of the anode by means of twelve equally spaced radial holes at the entrance to the plenum chamber (C). The gases mix within the plenum chamber and the hot air exits through the nozzle (D). All internal components of the arc are constructed of copper (except the tungsten cathode tip).

The two exit configurations shown in Fig. 1 were employed in the boundary layer experiments. The nozzle used to obtain the spatially resolved results had a rectangular cross-section 1/2 in. high by 1 in. wide. The ablating Teflon plate was positioned at the exit of the nozzle, flush with the bottom surface. For the far infrared experiments, where no spatial resolution was obtained, the nozzle cross-section was 3/4 in. diameter with a Teflon pipe insert. The latter configuration was used for the far infrared measurements to avoid the effects of Teflon surface radiation which could overwhelm the boundary layer radiation at these wavelengths.

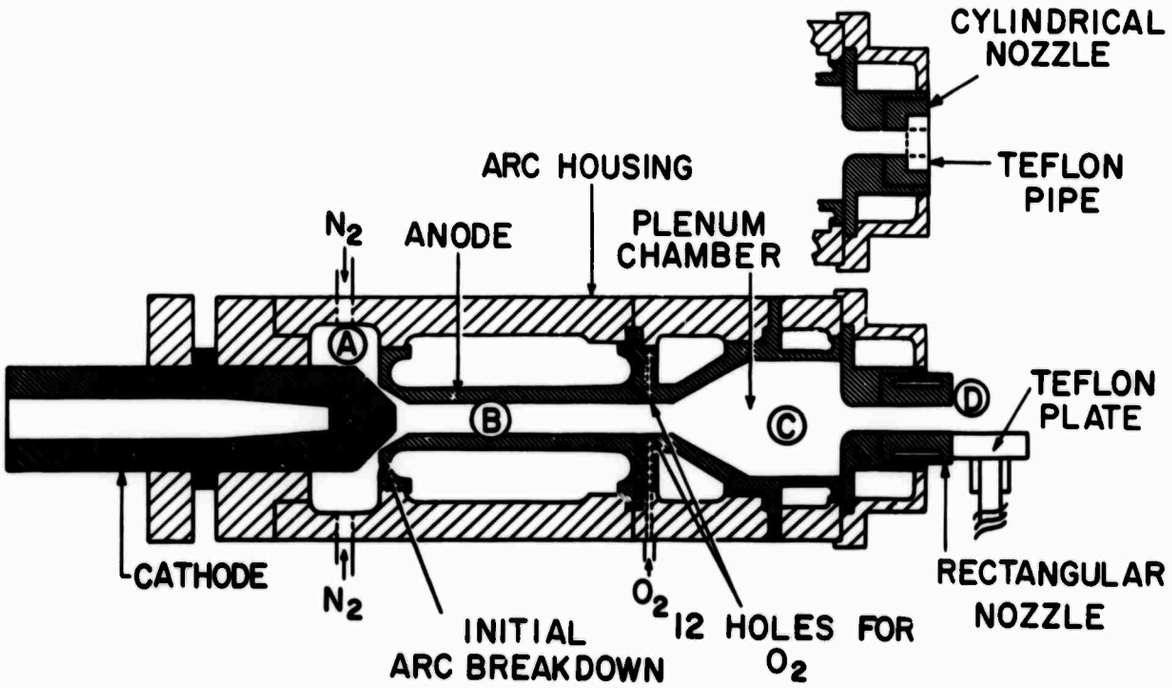

Fig. 1 Schematic diagram of the arc, showing the two nozzle configurations employed.

A3656

The stagnation enthalpy of the arc heated gas is determined by an energy balance, i.e., by measuring the power supplied to the arc, the power lost to the cooling water, and the flow rates of nitrogen and oxygen. The gas temperature is computed using the assumption of thermochemical equilibrium, which has been justified by the measurements discussed in Ref. 2 and 3.

Figure 2 shows schematically the optical configurations used for observation of the boundary layer. The external optical system, which had unit magnification, consisted of two 45^{o} mirrors, a 24 in. focal length spherical mirror and an aperture which served as a limiting stop. Visible spectra were obtained with a Hilger f/10 prism spectrograph and a Bausch and Lomb grating monochromator. With a 1/4 in. aperture, the spatial resolution is 0.13 mm. For the IR measurements a Perkin-Elmer Model #98 monochromator was used as a dispersion instrument. The radiation from the arc was chopped at about 1,000 cps just before entering this instrument (see Fig. 2). For the near infrared work the dispersed radiation exiting from the instrument was detected with a liquid nitrogen cooled indium antimonide cell which is sensitive from about 1μ to 5.5μ. For the far IR a copper-doped germanium detector sensitive in the range 2 - 18μ was used. The detector signal was passed through a narrow bandpass filter centered at the chopping frequency before being recorded on an oscilloscope. The electronics was such that the sensitivity of the system was limited by cell noise. The IR monochromator has equal entrance and exit slits which, of course, yields a triangular wavelength resolution function. The theoretical half width $\Delta\lambda$ of this resolution function for the calcium fluoride optics used here has been given by Strieff and Ferriso.[5] Experimental verification of

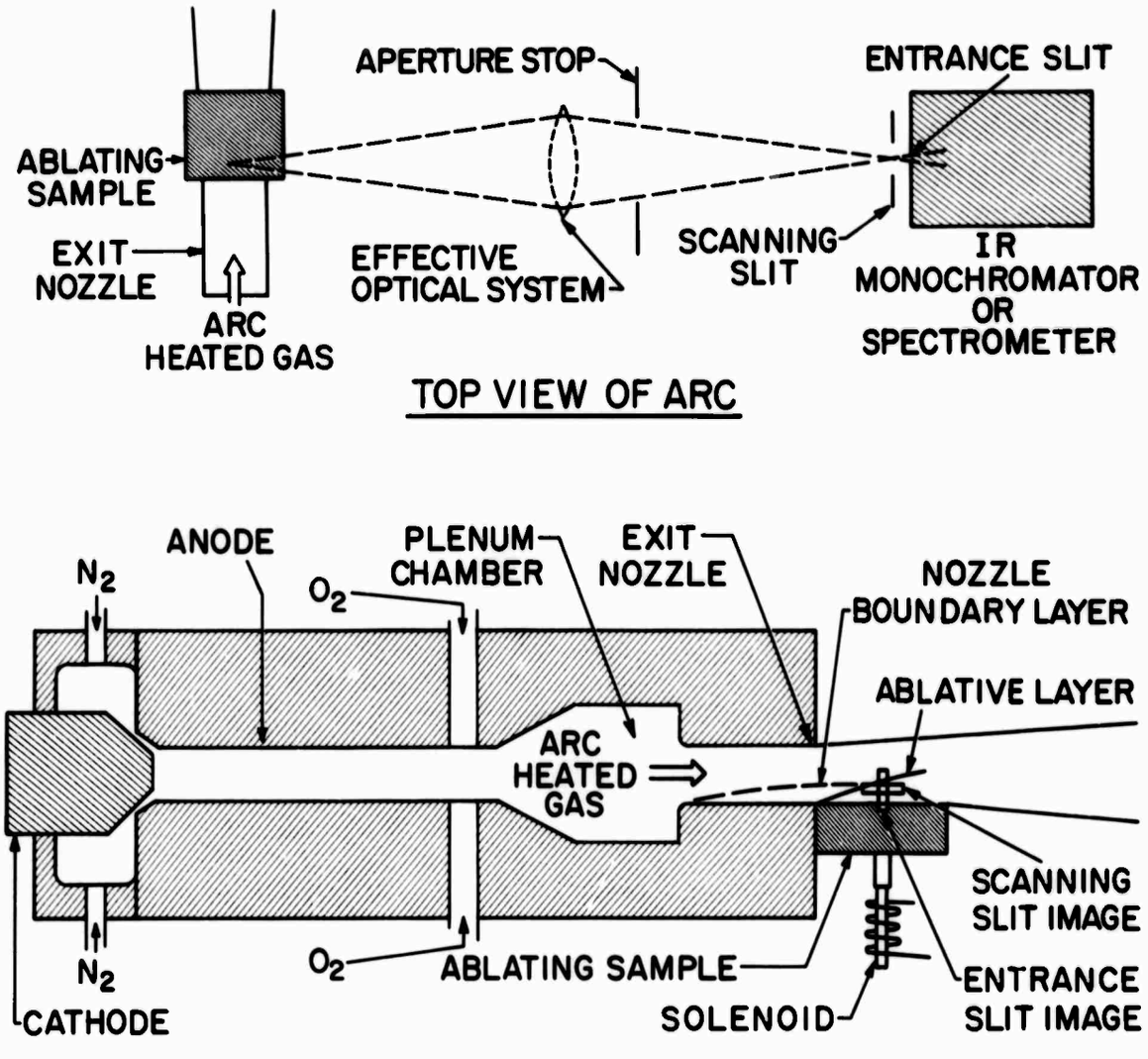

Fig. 2 Schematic diagram of optical configuration for the flat plate geometry. For the far IR experiments the monochromator slit was imaged at the centerline of the Teflon pipe 1.5 mm downstream from its exit.

the theoretical resolution function was carried out using several atomic lines in the IR. The wavelength calibration of the instrument was obtained between 1 and 12μ by using numerous IR standard absorption bands. Absolute intensity calibration of the entire optical system and detector was accomplished by employing a blackbody source at 500°C.

To obtain spatial resolution in the near IR a horizontal scanning slit was placed in front of the entrance slit to the monochromator. This slit was motor driven in a vertical direction as indicated in Fig. 2. The slit was imaged at the vertical plane of symmetry of the arc. In general, the width of this scanning slit was set at 0.25 mm, which was equal to the resolution of the external optical system. The slit was scanned at a velocity of 5 mm/sec, which was compatible with the bandpass of the electronic filter described above. Boundary layers are about 3 mm thick at a station 15 mm downstream from the leading edge of the Teflon block, where most of the measurements were carried out. The result of the geometry of the external optical system and the scanning slit is to produce a net spatial resolution of 0.5 mm in the near IR (1 - 5.5μ), which is one-sixth of a typical boundary layer thickness. Detailed radiation intensity profiles were measured at the following wavelengths: 3869 ± 33 Å, $2.48 \pm 0.18\mu$, and $2.90 \pm 0.24\mu$.

For the far IR measurements, where integrated radiation from the boundary layer formed in the Teflon pipe was measured, the entrance slit to the monochromator was imaged at the centerline of the pipe 1.5 mm downstream from its exit plane. Integrated radiation measurements spanned the 4 - 10μ region.

III. THEORY OF THE AIR-TEFLON BOUNDARY LAYER

The analysis of the ablating layer follows the lines of classical boundary layer theory except that detailed consideration must be given to the coupling between the ablating surface and the gaseous layer. Both energy and mass balances are made at this interface. Fortunately, the ablation temperature of Teflon is well known, so it is not necessary to construct a complete analysis of the heat transfer within the ablator to obtain a solution to the problem.

Assumptions and Governing Equations

We envisage a boundary layer in which all species have the same value of a given transport property, and all Lewis and Prandtl numbers are unity. Chemical nuclei rather than compounds are followed, which yields the simplification that the conservation of mass relation for each nucleus has no source term, since nuclei are neither created nor destroyed. Fick's law for the diffusion velocity is used. With these assumptions, the relative concentrations of the various nuclei can be obtained simply. Since all nuclei are assumed to have the same diffusivities, the oxygen/nitrogen ratio must be constant across the layer at its free stream value, 0.21/0.79. Similarly, for Teflon, $(C_2F_4)_n$, the carbon/fluorine ratio must be 1/2 across the layer. Thus, it is sufficient to determine only the mass fraction of the ablation material, C_A, across the layer. C_A is defined as

$$C_A = \sum_{\text{ablated}} \overline{C}_i = \overline{C}_C + \overline{C}_F , \qquad (1)$$

where $\overline{C}_i$ is the mass fraction of the ith nucleus. With brackets denoting the number of moles per mole of C_2F_4, we obtain the following expressions for the mole fractions:

$$[C] = 2\ ,\ [F] = 4$$

$$[O] = 1.47\ \frac{1 - C_A}{C_A}$$

$$[N] = 3.72\ [O] \tag{2}$$

The governing equations for conservation of momentum, energy, and ablating nuclei are written in terms of the Howarth-Dorodnitsyn independent variables ξ and η

$$\xi = \int_0^x u_e\,(\rho\mu)_w dx, \qquad \eta = \frac{u_e}{\sqrt{2\xi}} \int_0^x \rho\ dy \tag{3}$$

The subscript w denotes the wall value of $\rho\mu$, which is a function of ξ. We define the usual dependent variables as

$$f_\eta = \frac{u}{u_e}, \qquad g = \frac{H}{H_e} \tag{4}$$

where η (and ξ) subscripts are used to denote partial derivatives. In terms of these variables the conservation equations are:

momentum

$$f_{\eta\eta\eta} + f f_{\eta\eta} = 2\xi\,(f_\eta f_{\eta\xi} - f_\xi f_{\eta\eta}), \tag{5a}$$

energy

$$g_{\eta\eta} + f g_\eta = 2\xi\,(f_\eta g_\xi - f_\xi g_\eta), \tag{5b}$$

BLANK PAGE

ablating nuclei

$$C_{A\eta\,\eta} + fC_{A\eta} = 2\xi\,(f_\eta\, C_{A\xi} - f_\xi C_{A\eta}). \tag{5c}$$

The boundary conditions in the free stream are

$$g \to 1,\ f_\eta \to 1,\ C_A \to 0. \tag{6}$$

If we denote the location of the leading edge of the Teflon plate as ξ_o, the boundary conditions on the nozzle wall are, for $0 < \xi \leq \xi_o$

$$\eta = 0:\ \ g = g_{wo},\ f = 0,\ f_\eta = 0. \tag{7a}$$

The solutions to the governing Eqs. (5a, b) subject to these boundary conditions are the Blasius solution and the Crocco integral.

For $\xi > \xi_o$ we must perform energy and mass balances at the Teflon surface. The energy balance is obtained by first writing the net heat transfer from the gas to the surface, $-q_{Aw}$, as

$$-q_{Aw} = -q_w - (\rho v)_w h_w + (\rho v)_w h_{Aw}. \tag{7b}$$

Here $-q_w$ is the heat transfer by conduction and diffusion, and the other two terms represent convection of energy with the gas and ablator enthalpies respectively. For steady state ablation, $-q_{Aw}$ may also be written in terms of an energy balance within the solid Teflon:

$$-q_{Aw} = (\rho v)_w\,(h_{Aw} - h_{so}), \tag{7c}$$

where h_{so} is the enthalpy of room temperature solid Teflon. Eliminating q_{Aw} from the above equations yields the appropriate energy balance at the surface,

$$-q_w = (\rho v)_w\,(h_w - h_{so}). \tag{8}$$

The mass balance at the Teflon surface is

$$(\rho v)_w (1 - C_{Aw}) = -\mu \left(\frac{\partial C_A}{\partial y}\right)_w \tag{9}$$

In terms of the Howarth-Dorodnitsyn variables, the boundary conditions (8) and (9) are

$$\frac{g_{\eta w}}{g_{so} - g_w} = \frac{C_{A\eta w}}{1 - C_{Aw}} = f_w + 2\xi f_{\xi w}. \tag{10}$$

The Eqs. (5a, b, c) are a seventh order system with six boundary conditions, given by Eqs. (6), (7c) and (10). The additional boundary condition should involve a balance between the heat transfer within the ablator and its mass loss, which could determine the surface temperature. Since the ablation temperature of Teflon is known to be 1000°K within a few degrees, we employed this value as our additional boundary condition.

Thermodynamic Properties of the Air-Teflon Mixture

The solution of the system of equations and boundary conditions given above yields values for the enthalpy of the mixture and the mole fractions of C, F, O and N within the boundary layer. To compute the temperature and species profiles it is necessary to define a chemical model which determines the compounds formed by these elements. Previous results, discussed in detail in Refs. 2 and 3, have shown that the air radiation from both the free stream and nozzle boundary layer can be predicted within the experimental accuracy by equilibrium theories. For the ablation experiments, the assumption of concentration equilibrium for major species is reinforced by the rapid reactions between carbon compounds and oxygen.

The equilibrium composition may be computed by using a thermochemical equilibrium program, which is based on the JANAF tables.[6]

This procedure leads to a formidable complication at the wall where neither C_{Aw} or h_w are known, but T_w is well known for Teflon. The problem is to find values of C_{Aw} and h_w which satisfy both the equilibrium program, the boundary layer equations, and the interface conditions, Eq. (10).

It is instructive to consider a simple case to understand this complication. When g_w and C_{Aw} are dependent only on η and there is no nozzle boundary layer, the solutions to Eqs. (5b, c) are given by the Crocco integrals

$$\frac{C_{Aw} - C_A}{C_{Aw}} = \frac{g - g_w}{1 - g_w} = \frac{H - h_w}{H_e - h_w} .$$

These relations may be inserted into the boundary conditions given in Eq. (10) so that the following relation between h_w and C_{Aw} is obtained as a solution to the boundary layer equations at the wall

$$h_w = H_e - C_{Aw} (H_e - h_{so}). \tag{11}$$

The quantity h_{so} is the enthalpy of solid Teflon at 300°K. This enthalpy is obtained from Refs. 6-8 as -1.93 kcal/gm. Equation (11) is shown plotted in Fig. 3 for a free stream temperature of 6000°K as line A, which satisfies the boundary layer equations and the heat and mass balances at the surface. Calculations of h_w vs C_{Aw} using the equilibrium program based on Ref. 6 for a temperature of 1000°K and 1 atm are shown as line B in Fig. 3. The wall state should be at the intersection of these two lines, but they do not intersect. Raising the wall temperature to 1100°K would provide

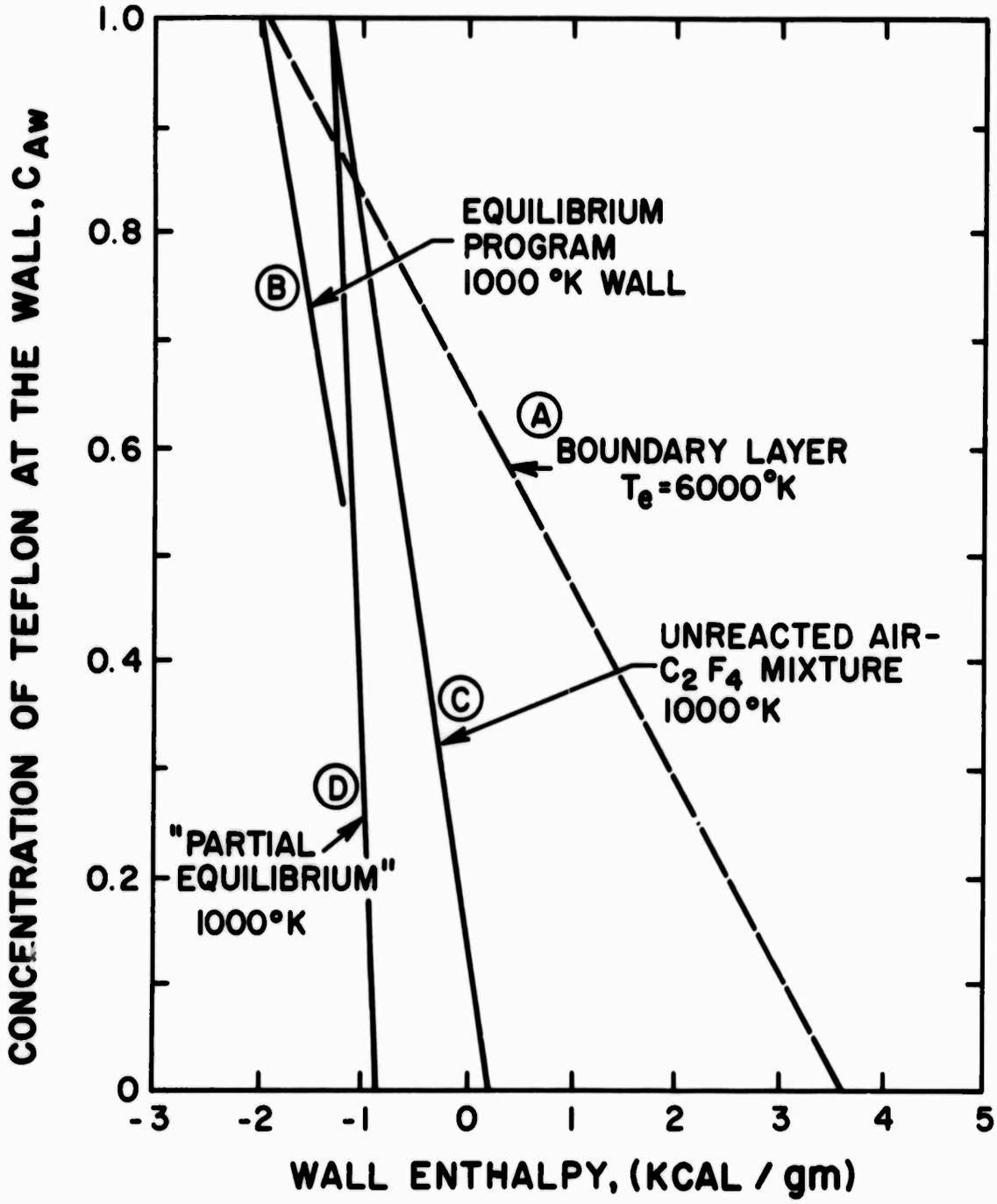

Fig. 3 Various chemical models of the wall state (solid lines) compared to a similar ablating boundary layer solution of the wall state (dashed line).

an intersection at $C_{Aw} = 1.0$; however, the composition of the gas for C_{Aw} near unity is largely CF_4, CF_3 and solid carbon. Since no continuum radiation from solid carbon was observed experimentally, the assumption of complete thermochemical equilibrium does not yield an acceptable picture of the gas state at the Teflon surface.

Another possible model for the thermodynamic state of the gas at the wall is an unreacted mixture of C_2F_4 gas and air, both at 1000°K and 1 atm. The results of such a mixture calculation are shown as line C in Fig. 3. Lines C and A do intersect, but if the values of C_{Aw} and h_w at the intersection are used in the equilibrium computations the resulting equilibrium state is at a temperature much greater than 1000°K because the C_2F_4 and O_2 react exothermically. This model would thus produce a temperature discontinuity at the wall, which is also unacceptable.

One way to reconcile the difficulties is to develop a model which predicts C_2F_4 gas at 1000°K as an equilibrium state if $C_{Aw} = 1$. This can be done by examining the kinetic model for C_2F_4 decomposition proposed in Ref. 9. Those results suggest that the equilibrium composition of curve B, which contains large amounts of CF_4 and CF_3, is not attained in the time scale of our experiments, since CF_3 and CF_4 are formed by three body processes which are relatively slow. We have, therefore, developed a "partial equilibrium" model in which the compounds CF_3 and CF_4 are deleted from the equilibrium calculation. The results of such a calculation are shown as curve D in Fig. 3. This curve maintains C_2F_4 gas at 1000°K when $C_{Aw} = 1.0$, and it crosses the boundary layer solution at a reasonable value of C_{Aw}. For C_{Aw} near unity, the gas is found to be a mixture of only

three compounds: C_2F_4, COF_2, and N_2; all the oxygen reacts with the C_2F_4 to form COF_2 and the N_2 is unreacted. This "partial equilibrium" model was used in the numerical calculations presented below.

For the three component mixture which is found at the wall, the enthalpy is a linear function of C_{Aw},

$$g_w = \frac{h_w}{H_e} = \frac{1}{H_e} (aC_{Aw} + b), \tag{12}$$

where a = 0.43 kcal/gm, and b = -0.857 kcal/gm. This relation is an analytical representation of the chemical state near the wall, which was utilized in the numerical solutions. Some of the details of the techniques used to obtain the numerical results are given in Ref. 3.

Theoretical Results

Theoretical calculations were performed for free stream temperatures of 3220, 4800 and 5800°K for comparison with the spatially resolved experiment (flat plate geometry), and at 3600, 4250 and 5400°K for comparison with the integral measurements (pipe geometry). For each set of cases the appropriate length of nozzle boundary layer run upstream of the Teflon sample was used. Since the results are qualitatively the same, only some representative examples will be shown.

The concentration of Teflon as a function of distance normal to the surface is illustrated for the pipe geometry in Fig. 4, along with corresponding temperature distributions. As expected, the Teflon concentration increases slightly with increasing free stream temperature. One feature of the temperature distributions is the plateau region about 0.2 - 0.5 mm from the surface. Of course, the enthalpy always increases monotonically

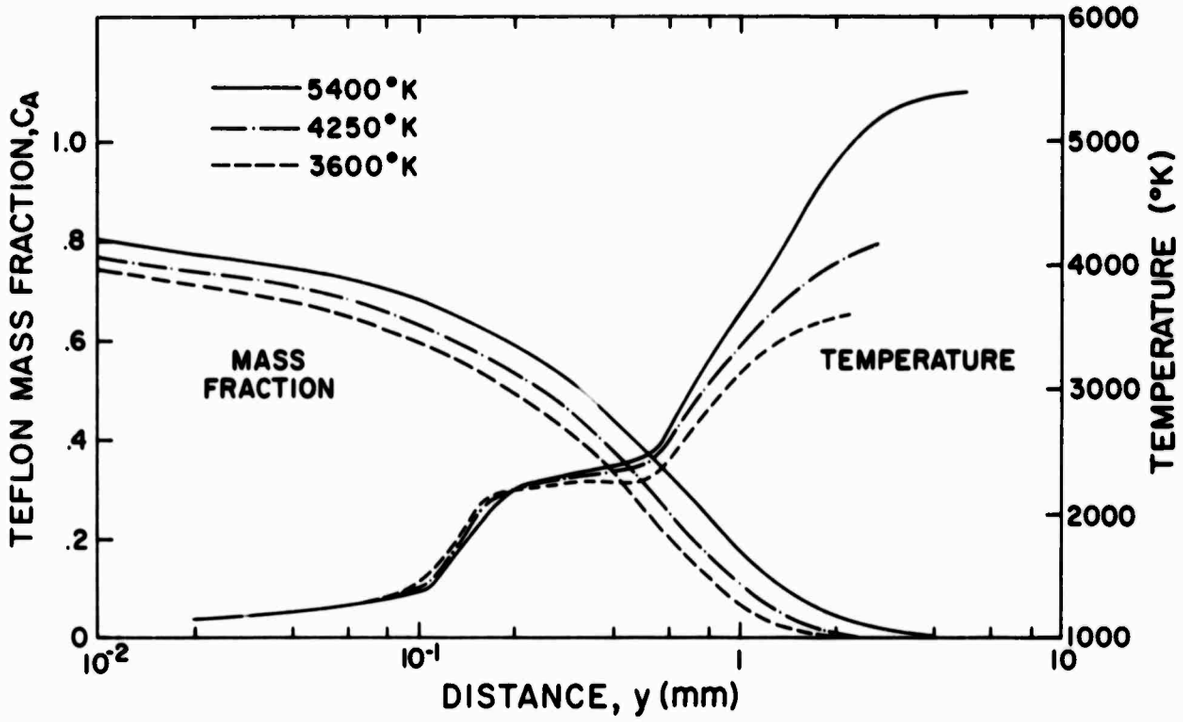

Fig. 4 Theoretical Teflon concentration and temperature profiles in the boundary layer at representative experimental free-stream temperatures.

from the surface in our model. Therefore, the plateau must be associated with endothermic chemical reactions occurring in this region of the layer. Figure 5 shows the distribution of reactants within the boundary layer $T_e = 4250^{\circ}K$. This result is illustrative of those obtained for the other temperatures. The temperature plateau region contains peaks in the particle density of F, CO and CO_2. Also, although the mass fraction of C_2F_4 is high at the wall, there are as many molecules of N_2 at the wall as C_2F_4 molecules. In addition, the particle concentration of COF_2 is high near the wall, but it decreases rapidly as we proceed out into the boundary layer.

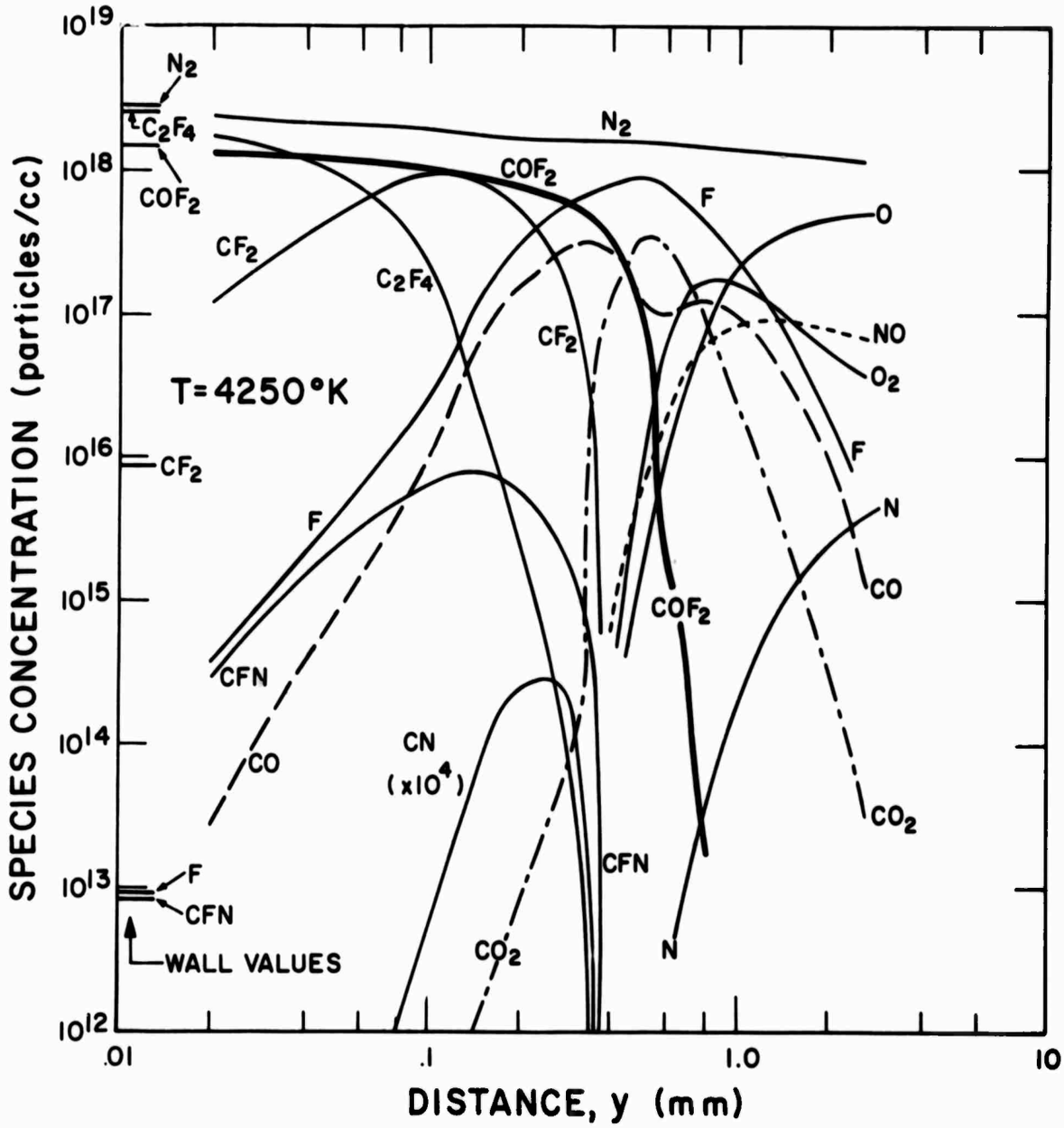

Fig. 5 Theoretical species concentrations within the boundary layer for a 4250°K free-stream temperature.

BLANK PAGE

IV. COMPARISON OF THEORY AND EXPERIMENT

An important qualitative feature of the experiments was the spectral identification of the principal radiators in the air-Teflon boundary layer. A spectrum of the boundary layer over a flat plate is shown in the lower portion of Fig. 6. The upper part of the spectrum is the arc heated air. Radiation in the visible and near UV is dominated by the CN violet system. Neither C nor C_2 (Swan) radiation was detected although some runs made with only nitrogen in the free stream showed them to be strong radiators in the nitrogen-Teflon boundary layer.

Spatially unresolved wavelength scans of the air-Teflon boundary layer between 2.0 and 3.2 μ indicated that the principal radiators were CO_2 $(\nu_1 + \nu_3)$, CO_2 $(2\nu_2 + \nu_3)$, NO (2ν) and CO (2ν). Of course, these scans also showed the NO (ν), CO (ν), and CO_2 (ν_3) bands in the 4.0 to 5.3 μ region. Although COF_2 was not identified in these scans, its possible presence in the spectra could not be eliminated. Additional scans in the far infrared confirmed the presence of COF_2. Although F atoms are a major component in part of the boundary layer according to the theory, they are not important radiators.

Theoretical predictions of temperatures and particle densities were combined with known radiation intensities in the experimental band-passes (see Appendix A) to determine the theoretical radiation profiles. These results will now be compared with experiment.

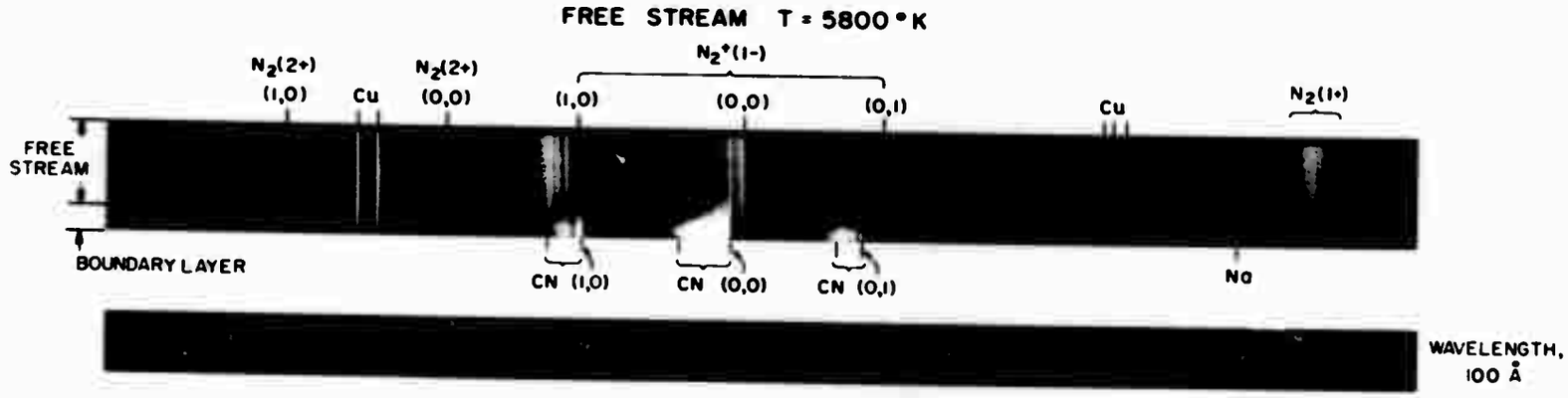

Fig. 6 Spectrum of free-stream air radiation (top) and spatially resolved spectrum of ablating boundary layer (bottom).

Near Infrared

Figure 7 shows the experimental and theoretical radiation profiles in the 2.90 ($\Delta\lambda$ = 0.24 μ) bandpass. The spatial resolution function of the optical instrument has been impressed on the theoretical profiles to provide a more accurate basis for comparison. The y = 0 position of the optical instrument was taken as the point where the leading edge of the resolution function first intersected the surface of the Teflon. However, the data are plotted using the position of the center of the resolution function. Therefore the radiation begins to rise at values of y less than zero. The peak in radiation is due to CO_2. At 5800°K NO contributes about 10% of the radiation. At 4800°K and 3220°K the NO radiation dominates in the outer portion of the boundary layer. The CO radiation contribution is always negligible in this bandpass. We see that both the peak intensity and its location are predicted well by the theory. However, beyond the peak, the theoretical predictions fall off more rapidly than the experimental data. As a result of this, the theoretical value for the total integrated radiation in this bandpass is about a factor of two lower than that obtained experimentally. The tail of the experimental boundary layer radiation curve in Fig. 8c is shown dotted since the accuracy of the measurement was poor in this region. More accurate measurements of the transition from boundary layer to free stream radiation showed good agreement with pure air free stream measurements. Note that the peak intensity of the CO_2 radiation in Fig. 7 is weakly dependent upon free stream temperature.

Figure 8 shows the radiation at λ = 2.48 μ ($\Delta\lambda$ = 0.18 μ) due to CO (2ν), COF_2 and IR Bremsstrahlung. Again the position and magnitude

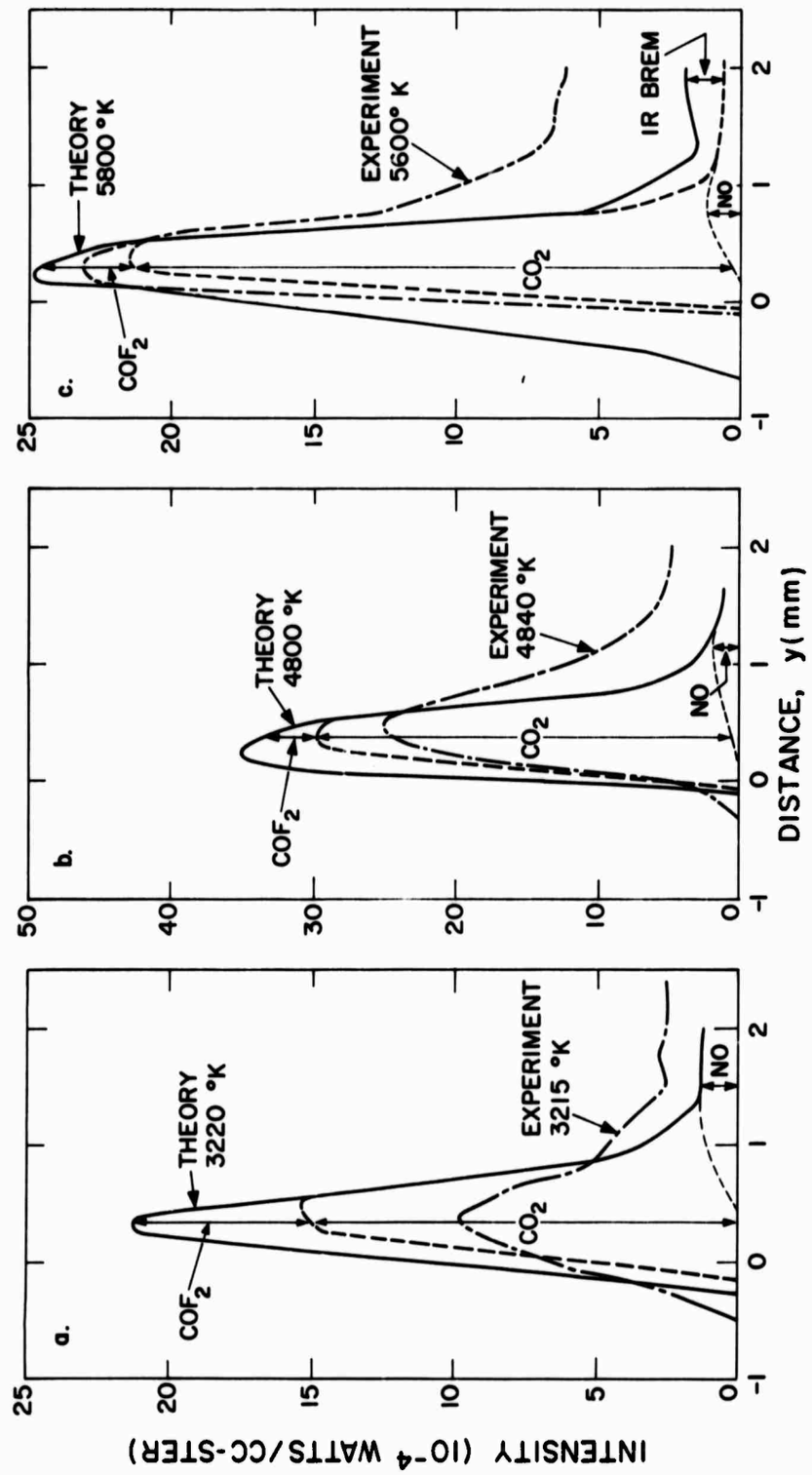

Fig. 7 Theoretical and experimental infrared radiation intensity distributions in the air-Teflon boundary layer in channel 1 ($\lambda = 2.90 \pm 0.24\ \mu$) for a flat plate.

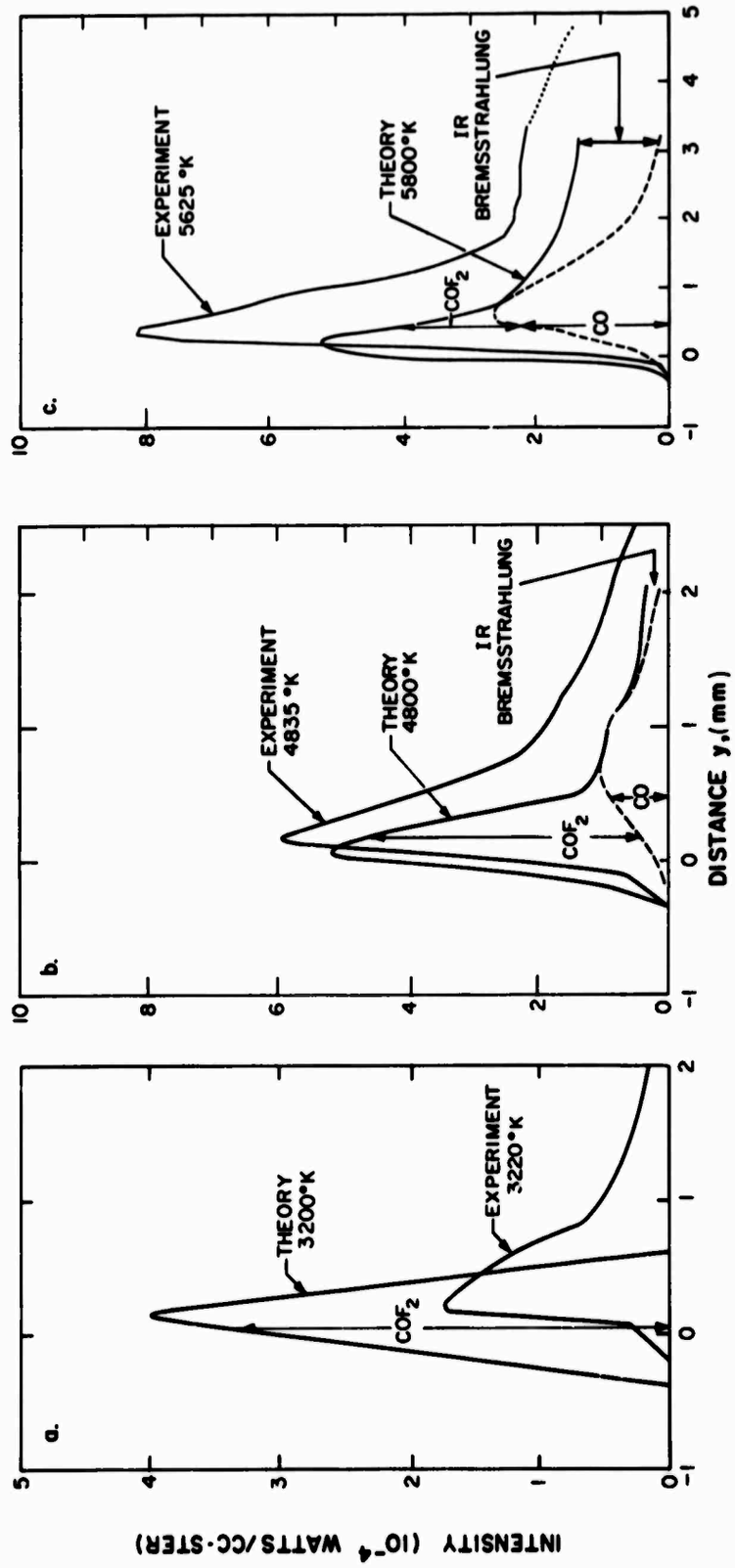

Fig. 8 Theoretical and experimental infrared radiation intensity distributions in the air-Teflon boundary layer; channel 2 ($\lambda = 2.48 \pm 0.18\,\mu$).

of the radiation peaks are predicted well. The COF_2 radiation predicted by the theory is highly peaked at the surface, and decays rapidly until it is negligible about 0.25 mm from the surface. The limited spatial resolution of the IR instrument did not permit us to positively identify the COF_2 radiation at this wavelength. At 3220°K the theory predicts that the most important radiator in the bandpass is COF_2. This radiation is about 10^2 times greater than the CO radiation.

Far Infrared

In the far IR increased emission from the Teflon surface prevented spatial resolution of the flat plate boundary layer, so integral measurements were made using the pipe geometry discussed earlier.

The air-Teflon spectra measured in the 8 μ region are illustrated in Fig. 9 for the case of free-stream temperatures near 3600°K. Three separate arc runs were used to cover the band; consistency between the three scans is very good. (Note that the irradiance corresponding to detector noise is greater at 10 μ than at 7 μ because of wavelength dependence of detector sensitivity.) At free-stream temperatures near 4200 and 5500°K, similar spectra were obtained; the peak is less pronounced at the higher temperatures.

To assist in the identification of this radiation, the spectral location of the centers of major fluorocarbon absorption bands are indicated in the figure. These bands are expected to be shifted to longer wavelengths from their band centers in emission at high temperature. The species CF, CF_4 and C_2F_2 can be excluded from major contribution to the observed spectral peak by consideration of their band locations. The 9 μ band of matrix-isolated CF_2 is stronger[10] than that at 8.2 μ, indicating

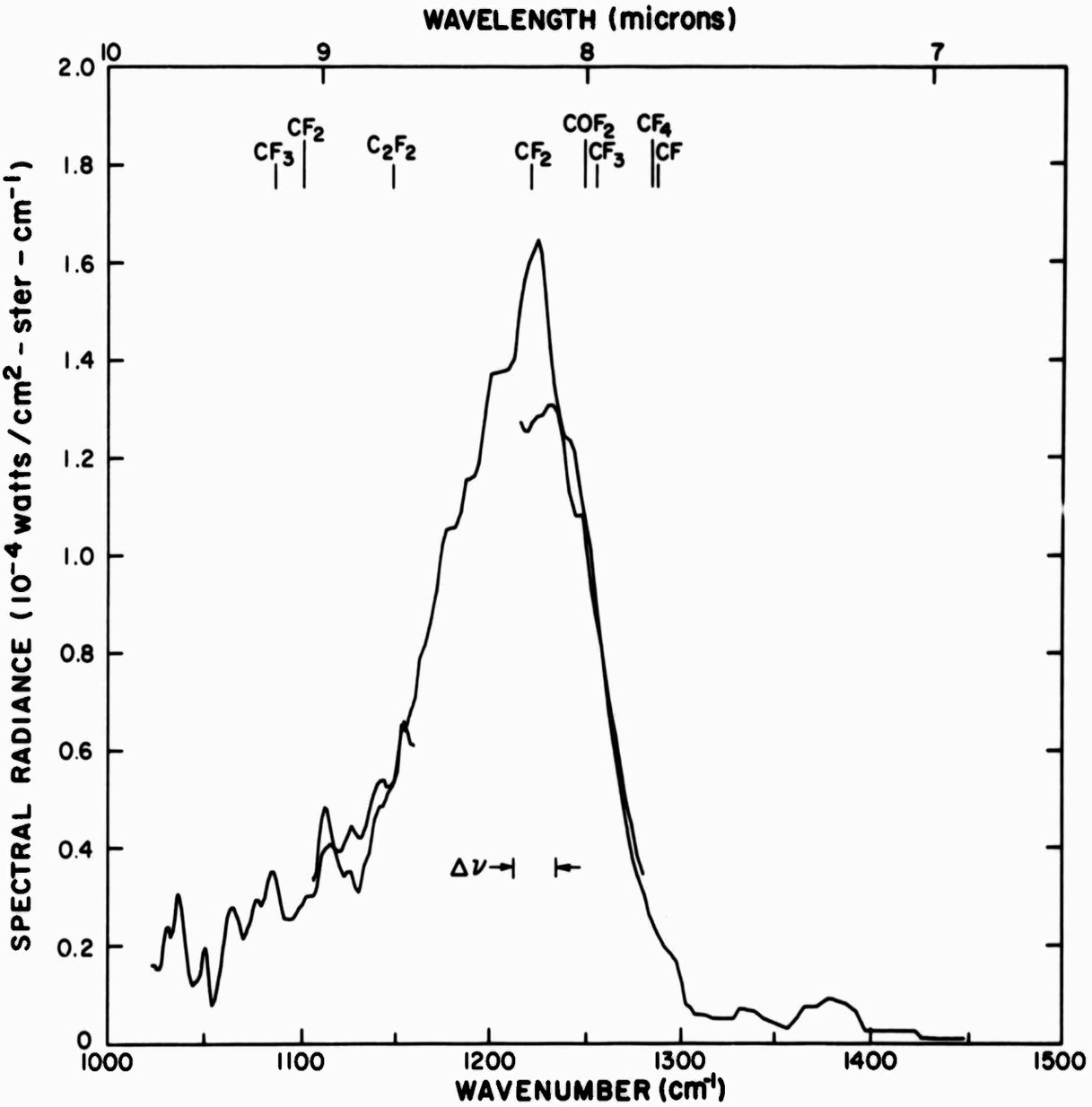

Fig. 9 Measured spectral intensity for free-stream temperatures near 3600°K. Absorption band centers are shown, as well as the full width at half height of the spectral resolution function, $\Delta\nu$.

that CF_2 radiation is not responsible for the radiation. This leaves the 8 μ bands of COF_2 and CF_3 as possibilities. We cannot exclude CF_3 on the basis of these observations alone, because its 9.2 μ band is weaker[10] in matrix isolation than that at 8 μ.

These observations may also be considered in the light of the boundary layer theory. Full equilibrium chemistry calculations predict a considerable amount of CF_3 and CF_4, and little COF_2; however, the very strong CF_4 7.8 μ band is not seen here in substantial amounts. Also, there is no indication of the 6.5 μ band of CF_4 in scans of that region. The partial equilibrium model presented above, which excludes CF_3 and CF_4, predicts that COF_2 will be the dominant radiator in the 5-10 μ region. This model gives a much better account of these observations.

The spectrally integrated intensity of the observed 8 μ band was determined for free stream temperatures of 3600, 4200 and 5500°K. The results are shown by the data points in Fig. 10. The predictions of the theory are given in the figure by the curves, which correspond to the two experimental values[11, 12] of the COF_2 band intensity. The data fall between these theoretical curves. The COF_2 radiation is predicted to come from the Teflon-rich, cool inner portion of the boundary layer, and its calculated intensity is very insensitive to the free-stream temperature. This flat temperature dependence is accurately confirmed by the measurements.

Spatially unresolved spectra are shown in Fig. 11 in the 4-6 μ region at free-stream temperatures near 3600°K. The 4.3 μ band of CO_2 appeared as expected; at 5.2 μ the COF_2 and NO bands are superimposed. Theoretical

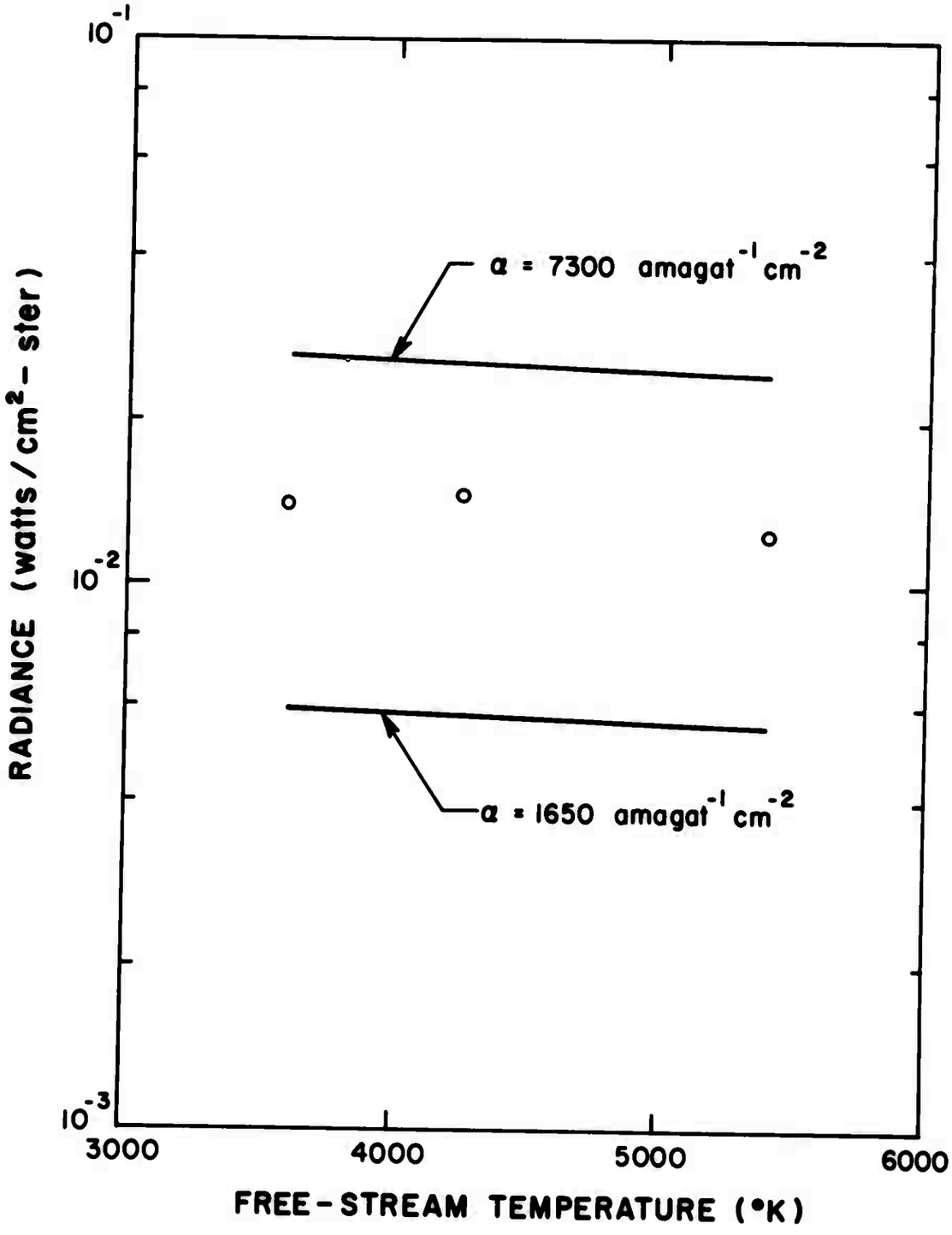

Fig. 10 Experimental data points and theoretical curves of the intensity of the 8μ COF_2 band.

predictions of the latter radiation intensities are shown in Table I. COF_2 is seen to be the dominant boundary layer radiator at 5.2 μ, although the free-stream NO radiation contributes one-third of the predicted total. For comparison, the spectrum on Fig. 11 was integrated to obtain the measured 5.2 μ band intensity shown in the table. The agreement is excellent - better, in fact, than the probable error of either theory or experiment.

TABLE I

AIR-TEFLON RADIATION AT 5.2 μ

	Band intensity (watts/ster-cm^2)
Calculated:	
COF_2	1.06×10^{-2}
NO boundary layer	.08
NO free stream	.45
Total	1.59×10^{-2}
Measured:	1.48×10^{-2}

Visible Radiation

The CN (violet) radiation is shown for the T = 5800 and 4800°K in Figs. 12 and 13. At 5800°K the peak and total intensity are predicted well, but the location of the peak is twice as far from the surface as the experimental measurement. Also, the second peak near the surface is not predicted. At 4800°K the theory predicts no radiation peak; in fact, the dominant radiator is predicted to be NO (β). The 3200°K result, not shown here, is similar to the 4800°K case.

Since the dissociation energy of 7.5 ev for CN is recommended in Ref. 6 with reservations, and is somewhat controversial, we also calculated

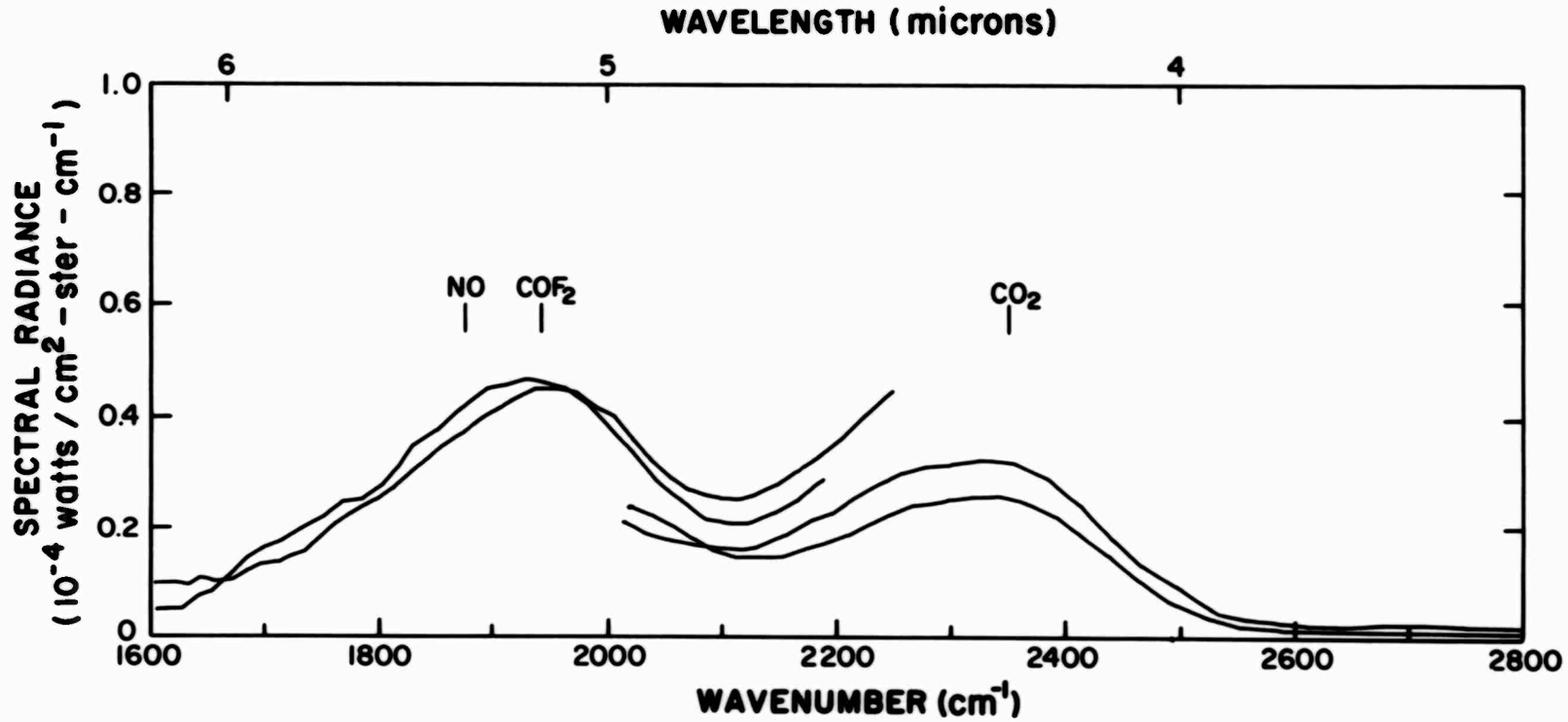

Fig. 11 Measured spectral intensity for free-stream temperatures near 3600°K.

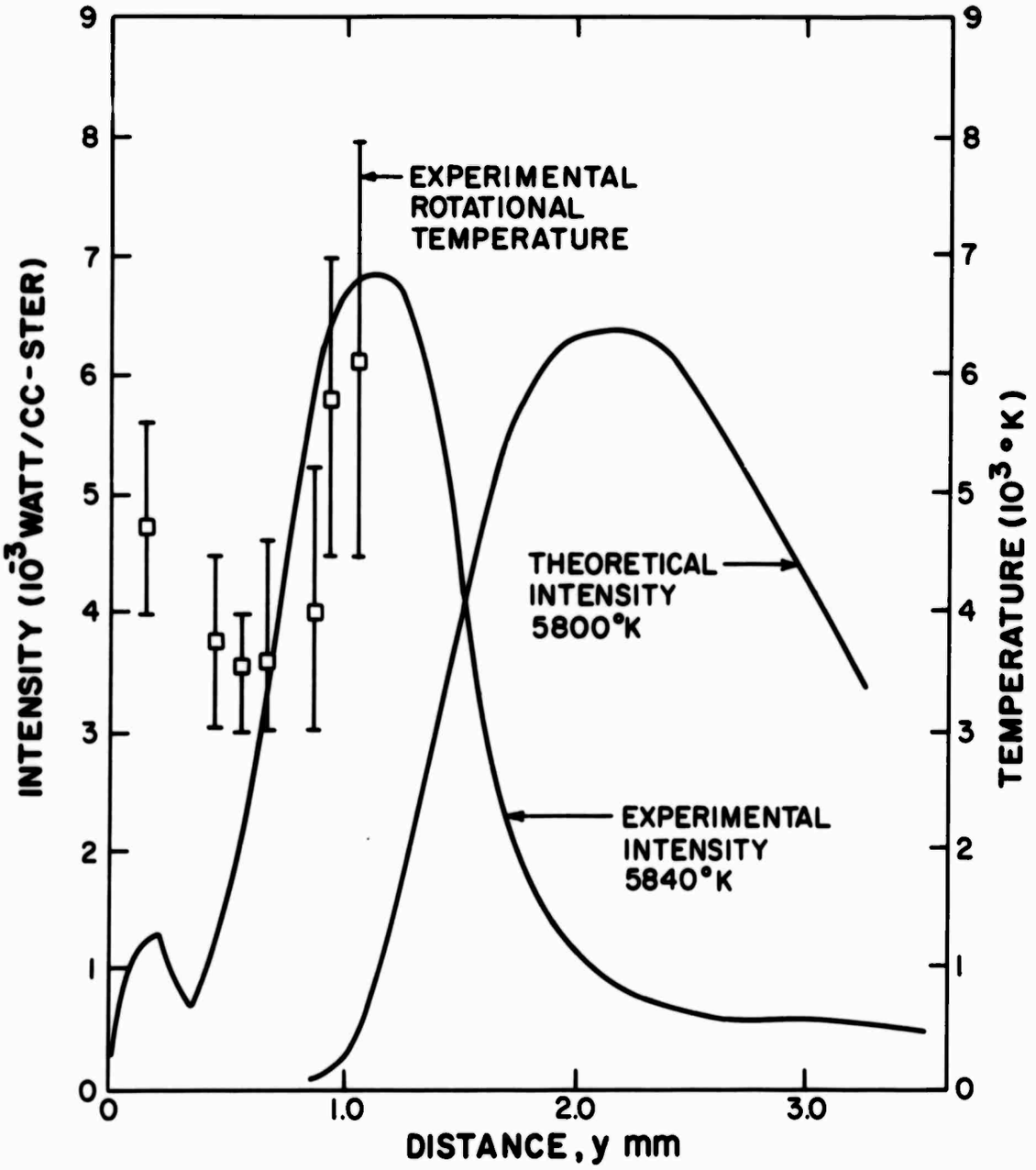

Fig. 12 Visible radiation in the air-Teflon boundary layer, and experimental rotational temperature distribution.

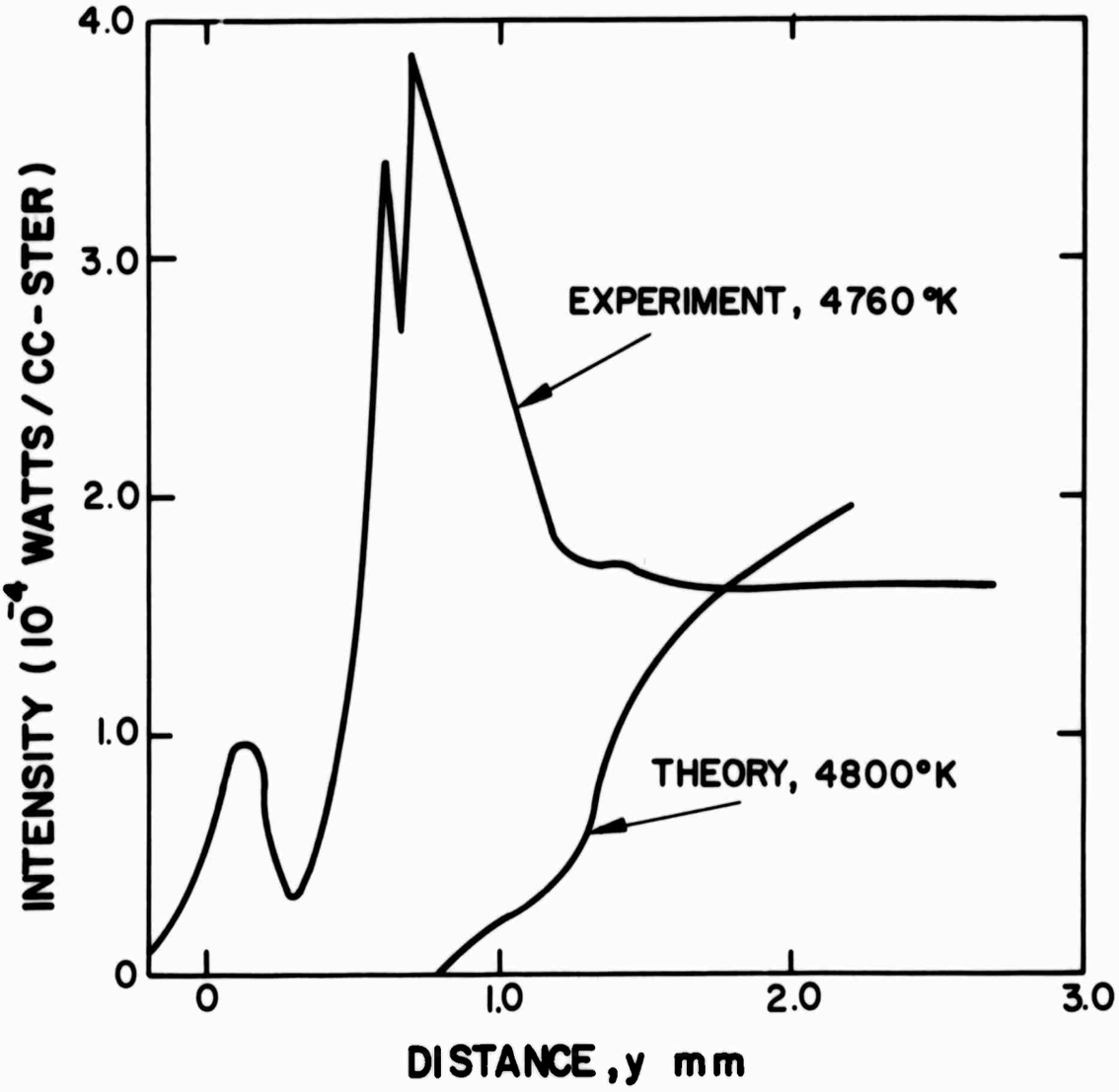

Fig. 13 Visible radiation in the air-Teflon boundary layer.

the "partial equilibrium" concentrations, temperatures, and the resulting radiation for $T_e = 5800^{\circ}K$ using a value of 8.1 ev for the dissociation energy of CN. Since CN is a trace species in the boundary layer, the temperature is essentially unaffected by the different dissociation energy; however, the CN concentration increases by a factor of three. The CN radiation is increased by this same factor over that shown in Fig. 12, but the shape of the theoretical curve is unchanged. At lower temperatures the increased dissociation energy does not increase the CN radiation significantly.

Also shown in Fig. 12 is the CN (violet) (0, 0) rotational temperature profile in the boundary layer, which was obtained by densitometry of a spectral plate.[2] It may be compared with the calculated temperature distributions shown in Fig. 4. At the outer edge of the boundary layer the rotational temperature agrees reasonably well with the calculated temperature. However, instead of decreasing monotonically to the wall temperature, the rotational temperature rises to over $4000^{\circ}K$ near the Teflon surface.

This effect is presently unexplained in detail, but might be due to formation of the electronically excited state of CN ($B^2\Sigma$) in high rotational levels which radiate before they can be quenched by collisions. Such a phenomenon is well documented in the flame spectroscopy literature; for example, the OH radical has yielded rotational temperatures well above the theoretical equilibrium flame temperature.[13] CN, like OH, has a very short radiative lifetime. Kiess and Broida[14] have found anamolous rotational distributions in the CN (violet) radiation from "cold" flames of atomic nitrogen reacting with halogenated hydrocarbons.

The "partial equilibrium" model was utilized in the theoretical calculations since it gave a physically acceptable temperature and chemical composition at the wall. However, while use of the full equilibrium model at the wall resulted in temperature discontinuities, the radiation predictions further out in the boundary layer were quite similar to those obtained with the "partial equilibrium" model.

BLANK PAGE

V. CONCLUSIONS

A simple theory of the ablating Teflon-air boundary layer has been constructed which is capable of accurately predicting detailed radiation profiles. The predictions have been compared with measured radiation, both spatially resolved and spatially integrated. This is a stringent test of any theory since the radiation is strongly dependent on both the temperature and species concentration profiles, and so is much more sensitive than such gross properties as heat transfer, skin friction, or ablation rate. However, the degree of success achieved by such a theory is a good test of an understanding of the aerothermochemical processes in an ablating boundary layer, since the fluid mechanics and chemistry are closely coupled and both play important roles in determining the results.

The approach has been to construct the simplest theory which contains all the features thought to be important in the description of the physical processes. Thus the complete heat and mass balances at the ablating wall have been included along with the non-similar effect of the boundary layer on the arc nozzle into which the ablating layer grows. The close coupling of the fluid mechanical and chemical processes has led to the use of a "partial equilibrium" chemical model which suppresses the species CF_3 and CF_4, which we believe form too slowly to play a role in the ablating layer. On the other hand, the fluid mechanics has been simplified by taking the various transport properties of all species the same, and dealing only with unit values of the Prandtl and Lewis numbers.

This has enabled us to treat the problem with only a moderate amount of computational difficulty in spite of the non-similarity and the coupled boundary conditions.

The theory so constructed is able to predict the peak intensity of the 2.9μ CO_2 radiation, its position in the boundary layer and its integrated intensity across the layers. The peak CO_2 radiation is independent of temperature in the range of our experiments, 3200-6000°K.

At 2.48μ, the radiation peak is also predicted well, and the theory suggests that most of this radiation is from COF_2. However, the individual contributions from COF_2 and CO could not be distinguished experimentally at this wavelength because of spatial resolution limitations.

To check these predictions of high COF_2 concentration within the ablating layer, spatially unresolved radiation measurements were made in the 4-10μ region. The spectral measurements confirmed the presence of COF_2. Furthermore, integration of the spectra showed agreement with the theoretical model within the uncertainty of the value for the integrated band intensity of COF_2 at 8μ. At 5.2μ the data also fits the model, if the effect of NO radiation is taken into account.

Thus the measurements confirm the hitherto unsuspected presence of substantial amounts of COF_2 in the Teflon-air boundary layer, which is predicted by the partial equilibrium chemical model. This gives strong support to this model, which was originally found necessary to enable proper coupling of the fluid mechanics and chemistry near the ablating surface.

The theory is unable to predict the visible CN radiation data with accuracy comparable to that found for the infrared radiation. In addition, an anomalous CN rotational temperature was measured, peaking near the wall. This leads us to conclude that even at one atmosphere, the dominant visible and near UV radiation in the Teflon-air boundary layer comes from the trace species CN which is not in thermodynamic equilibrium with the major energy containing species.

It appears that the simple theory constructed here, which led to the necessity of using a partial equilibrium chemical model, is capable of predicting many of the major features of the radiation from the ablating Teflon-air boundary layer. It has enabled prediction of IR radiation from COF_2 which was then experimentally observed to be in both qualitative and quantitative agreement with the predictions. The lack of ability to predict visible CN radiation has suggested that this species is not in equilibrium.

VI. ACKNOWLEDGMENT

The authors would like to acknowledge the assistance of R. Castano, G. Caledonia and H. Koritz in the experimental program. During the course of this investigation, many fruitful discussions were held with M. Camac and G. W. Sutton.

APPENDIX A

THEORETICAL RADIATION INTENSITIES

The near infrared radiation intensities per particle were calculated for the $2.90 \pm 0.24\mu$ and $2.48 \pm 0.18\mu$ band passes by the following technique. The IR intensity transmitted by the monochromator is

$$I = \int I(\lambda)\, R(\lambda)\, d\lambda$$

where $I(\lambda)$ is the spectral intensity of a molecular band in watts/ster-particle - μ and $R(\lambda)$ is the triangular resolution function of the monochromator. Also,

$$I(\lambda) = \frac{N_\lambda}{L_o} \frac{S}{d}$$

where N_λ is the blackbody spectral radiance in watts/cm^2-ster-μ, L_o is Loschmidt's number and S/d is the spectral absorption coefficient in amagat^{-1} cm^{-1} (S is the integrated intensity of each spectral line and d is the spacing between lines.) The spectral absorption coefficient S/d for the CO_2 2.7μ band was obtained from a calculation by Malkmus.[15] His calculations were made for temperatures of 300, 600, 1200, 1500, 1800, 2400 and 3000°K. We extrapolated his spectra to 3600 and 4200°K, judging the spectral distribution by eye and adjusting the integral for agreement with the expected temperature dependence.[16] The absorption coefficients for CO were obtained from Ref. 17. For the CO 2.35μ band, an integrated band intensity of 1.88 amagat^{-1} cm^{-2} at room temperature was used. The NO spectra were calculated by methods similar to those

of Ref. 17, and were based on a band intensity of 2.4 amagat^{-1} cm^{-2} at room temperature. The results of all of these IR calculations are shown in Fig. 14.

The neutral Bremsstrahlung radiation intensity in the IR was computed from the equation[18]

$$I(\lambda) = 1.63 \times 10^{-39} \lambda^{-2} T^{-1/2} \exp(-1.438/\lambda T)[n_e] \sum_i Z_i^2 [n_i]$$

where Z_i is the "effective coulombic charge" of the neutral scattering species n_i, and the summation is over all these species. The effective Z^2 for the relevant species were taken to be[18] $Z^2_{N_2} = 2.2 \times 10^{-2}$, $Z^2_N = 0.9 \times 10^{-2}$, and $Z^2_O = 0.2 \times 10^{-2}$.

The intensity per molecule of the COF_2 and NO bands in the 5-8 μ region was calculated from the integrated band absorption coefficient, a, by means of the expression

$$I = a N^o_\nu / L,$$

where N^o_ν is the blackbody radiance. Table II lists the values of a employed. Band intensities Γ(cm^2/mole) found in reference 11 were converted by means of the relationship

$$a = \nu \Gamma / V_o$$

where ν is the wave number of the band center. Since we are concerned here with fundamental bands, a may be taken as constant with respect to temperature in the above equation. The results of these calculations are shown in Fig. 15. Note that two curves are shown for the 8μ band of COF_2, corresponding to the two values of integrated absorption coefficient obtained from references 11 and 12.

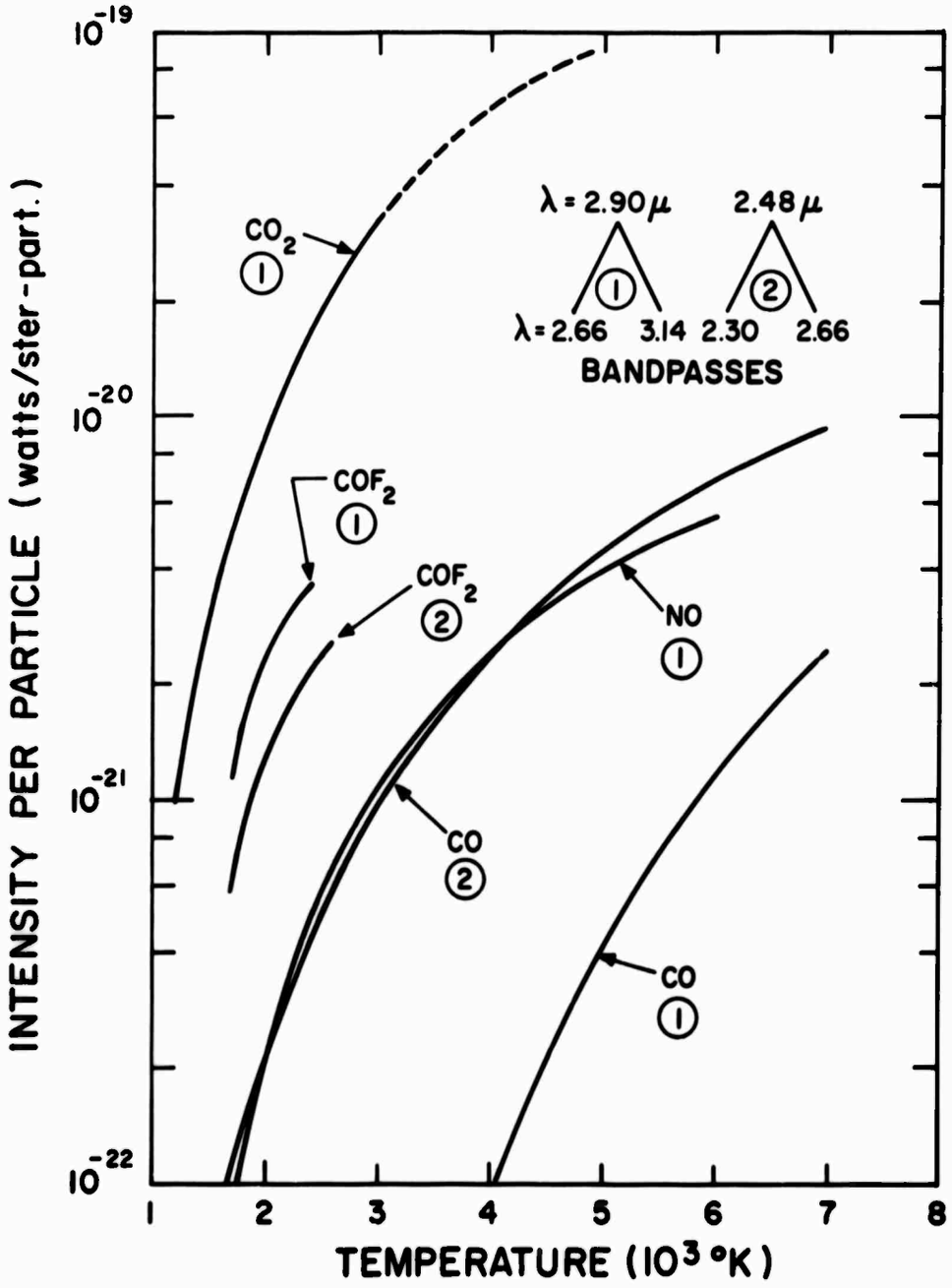

Fig. 14 Radiation intensities per particle in the various bandpasses studied.

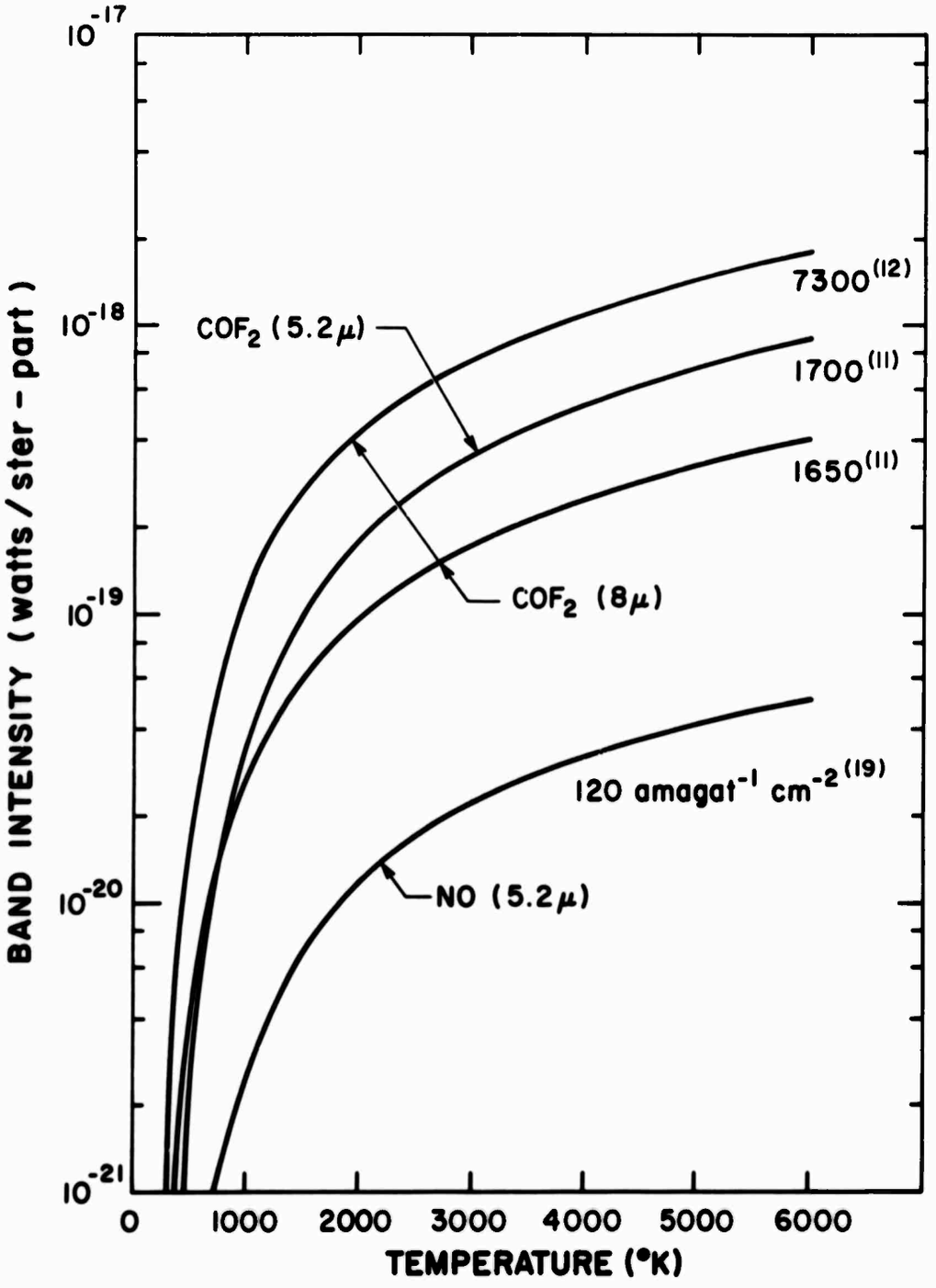

Fig. 15 Emission intensities of various infrared bands. Each curve is labeled by the value of the integrated band absorption coefficient used, and by reference number.

TABLE II

Integrated absorption coefficients, a

Species	Band	a (amagat^{-1} cm^{-2})	Reference
COF_2	8.0μ	1650	11
		7300	12
	5.2μ	1700	11
NO	5.2μ	120	19

To compare with the experimental measurements of visible radiation, we calculated the radiation in the spectral band of 3869 $\pm$ 33 Å. The significant radiators in this region are CN (violet), O_2(SR), NO (β), N_2^+(1-), N_2(2+), and O^- free-bound. The relations used for predicting the radiation (watts/cm^3 -ster) in terms of the temperature T($^\circ$K) and concentrations [ ] (particles/cm^3) are the following:

$$\underline{\text{CN(violet)}}: \qquad \frac{4.8 \times 10^{-13} [\text{CN}] \exp(-37,200/T)}{1+2.5 \exp(-13,100/T)}$$

$$\underline{\text{O}_2\text{(SR)}}: \qquad \frac{1.8 \times 10^{-30} [\text{O}_2] \exp(-71,000/T)}{T[1+0.67 \exp(-11,300/T)]} \int \phi \lambda^{-6} d\lambda$$

$T \times 10^{-3}$:	2	3	4	5	6
$10^{-19} \int \phi \lambda^{-6} d\lambda$:	4.1	5.8	7.3	8.4	9.4

$$\underline{\text{NO}(\beta)}: \qquad 3.46 \times 10^{-31} T^{-1} [\text{NO}] \int \phi \lambda^{-6} d\lambda \exp(-65,400/T)$$

$T \times 10^{-3}$:	2	3	4	5	6
$10^{-19} \int \phi \lambda^{-6} d\lambda$:	3.5	4.5	5.4	6.2	6.8

$$\underline{N_2^+(1-)}: \qquad \frac{2.3 \times 10^{-30} [N_2^+] \exp(-36,800/T)}{T[1+2.45 \exp(-12,700/T)]} \int \phi \lambda^{-6} d\lambda$$

$T \times 10^{-3}$: 2 3 4 5 6

$10^{-20}\int \phi \lambda^{-6} d\lambda$: 2.5 3.2 3.5 3.6 3.6

$\underline{N_2(2+)}$: $3.13 \times 10^{-29} [N_2] T^{-1} \int \phi \lambda^{-6} d\lambda \exp(-128,000/T)$

$T \times 10^{-3}$: 3 4 5 6

$10^{-19}\int \phi \lambda^{-6} d\lambda$: 1.0 1.8 2.5 3.2

$\underline{O^-(fb)}$: $6.5 \times 10^{-14} [O^-] \exp(-37,200/T)$

The CN (violet) radiation equation is based on a radiative lifetime of 8.5×10^{-8} sec.[20] Since most of the CN (violet) radiation is in the $\Delta v = 0$ sequence which lies within the above bandpass this simple equation is sufficiently accurate. The radiation equations for the O_2(SR), NO (β), N_2^+ (1-) and N_2(2+) systems are based on the electron transition probability for each system[21] evaluated at 3869 Å. The theoretical equation for the radiation was obtained from Ref. 22. The detailed shape of the spectrum is given by ϕ which is weighted by λ^{-6} in integrating over the band.[22] The values given above for $\int \phi \lambda^{-6} d\lambda$ also include the resolution function of the optical instrument used in the experimental work. Values of $\phi\lambda^{-6}$ as a function of λ over a range of temperatures for the radiating systems of interest are given in Ref. 23. For all of the above radiators, all of the excited electronic states were assumed to be in equilibrium with the ground state. The O^-(fb) radiation was calculated from a theoretical equation given in Ref. 21 using the photodetachment cross section for O^- measured by Branscomb, et al.[24]

REFERENCES

1. Wray, K. L., Rose, P. H. and Koritz, H. E., "Measurements of the Radiation from an Ablation Contaminated Boundary Layer Under Simulated Flight Conditions", Avco Everett Research Laboratory Research Report 226, August 1965.

2. Wray, K. L. and Kemp, N. H., "The Ablating Boundary Layer on a Teflon Plate in an Arc-Heated Air Stream", Avco Everett Research Laboratory Research Note 596, August 1966; AIAA Paper No. 56-66, January 1966.

3. Greenberg, R. A., Kemp, N. H. and Wray, K. L., "Structure of the Laminar Ablating Air-Teflon Boundary Layer", Avco Everett Research Laboratory Research Report 301 (November 1968); AIAA Paper No. 69-99 (January 1969), (to be published in the AIAA Journal).

4. Young, L. A., Greenberg, R. A. and Wray, K. L., "COF_2 Radiation from an Ablating Air-Teflon Boundary Layer", Avco Everett Research Laboratory Research Report 330, June 1969. (To be published in J. Quant. Spect. Radiat. Transf.)

5. Strieff, M. L. and Ferriso, C. C., "Spectral Slit Width of a Small Prism Monochromator", GDA-DBE64-054, General Dynamics/ Astronautics Space Science Laboratory, San Diego, California, August 1964.

6. "JANAF Thermochemical Tables", The Dow Chemical Company, Midland, Michigan.

7. Wentink, T., "High Temperature Behavior of Teflon", Avco Everett Research Laboratory Research Report 55, July 1959.

8. Settlage, P. H. and Siegle, J. C., "Behavior of Teflon Fluorocarbon Resins at Elevated Temperatures", Planetary and Space Science 3, 73-81 (1961).

9. Modica, A. P. and Sillers, S. J., "Experimental and Theoretical Kinetics of High Temperature Fluorocarbon Chemistry", J. Chem. Phys. 48, 3283-3289 (1968).

10. Milligan, D. E. and Jacox, M. E., "Matrix-Isolation Study of the Reaction of Atomic and Molecular Fluorine with Carbon Atoms. The Infrared Spectra of Normal and ^{13}C-substituted CF_2 and CF_3", J. Chem. Phys. 48, 2265-2271 (1968).

11. Hopper, M. J., Russell, J. W. and Overend, J., "Vibrational Intensities. XVI. COF_2, $COCl_2$, and $COBr_2$", J. Chem. Phys. 48, 3765-3772 (1968).

12. Thompson, W. P., Bott, J. F., and Jacobs, T. A., Aerospace Corp., Private communication.

13. Gaydon, A. G., "The Spectroscopy of Flames", (Chapman and Hall, Ltd., London, 1957) Chap. VIII.

14. Kiess, N. H. and Broida, H. P., "Seventh Symposium on Combustion", (Butterworth Publications, London, 1959) p. 207.

15. Malkmus, W., "Infrared Emissivity of Carbon Dioxide (2.7μ band)", J. Opt. Soc. Am. 54, 751-758 (1964).

16. Breeze, J. C., Ferriso, C. C., Ludwig, C. B., and Malkmus, W., "Temperature Dependence of the Total Integrated Intensity of Vibrational-Rotational Band Systems", J. Chem. Phys. 42, 402-406 (1965).

17. Young, L. A., "CO Infrared Spectra", J. Quant. Spec. Radiat. Transf., 8, 693-716 (1968).

18. Taylor, R. and Caledonia, G., "Experimental Determination of the Cross-Section for Neutral Bremsstrahlung II. High Temperature Air Species - O, N and N_2." J. Quant. Spect. Radiat. Transfer 9, 681-696 (1969).

19. Varanasi, P. and Penner, S. S., "Absolute Intensity Measurement of the Fundamental of NO", J. Quant. Spect. Radiat. Transfer 7, 279-282 (1967).

20. Fairbairn, A., "Spectrum of Shock-Heated Gases Simulating the Venus Atmosphere", AIAA J. 2, 1004-1007 (1964).

21. Keck, J. C., Allen, R. A., and Taylor, R. L., "Electronic Transition Moments for Air Molecules", J. Quant. Spect. Radiat. Transf 3, 335-353 (1963).

22. Keck, J. C., Camm, J., Kivel, B., and Wentink, T. Jr., "Radiation from Hot Air. Part II", Annals of Phys. 7, 1-38 (1959).

23. Allen, R., "Air Radiation Tables: Spectral Distribution Functions for Molecular Band Systems", Avco Everett Research Laboratory Research Report 236, April 1966.

24. Branscomb, L. M., Burch, B. S., Smith, S. J., and Geltman, S., "Photodetachment Cross Section and the Electron Affinity of Atomic Oxygen", Phys. Rev. 111, 504-513 (1958).

UNCLASSIFIED

Security Classification

DOCUMENT CONTROL DATA · R&D

(Security classification of title, body of abstract and indexing annotation must be entered when the overall report is classified)

1 ORIGINATING ACTIVITY (Corporate author) Avco Everett Research Laboratory 2385 Revere Beach Parkway Everett, Massachusetts	2a REPORT SECURITY CLASSIFICATION Unclassified 2b GROUP

3 REPORT TITLE

Radiation From Air-Teflon Boundary Layers

4 DESCRIPTIVE NOTES (Type of report and inclusive dates)

AMP 294

5 AUTHOR(S) (Last name, first name, initial)

Greenberg, R. A., Wray, K. L. Young, L. A. and Kemp, N. H.

6 REPORT DATE	7a TOTAL NO. OF PAGES	7b NO. OF REFS
March 1970	52	24

8a CONTRACT OR GRANT NO. F04701-68-C-0036	9a ORIGINATOR'S REPORT NUMBER(S) AMP 294
b PROJECT NO	
c	9b OTHER REPORT NO(S) (Any other numbers that may be assigned this report) SAMSO-TR-70-44
d	

10 AVAILABILITY/LIMITATION NOTICES

Distribution of this document is unlimited. This indicates document has been cleared for public release by competent authority.

11 SUPPLEMENTARY NOTES	12 SPONSORING MILITARY ACTIVITY Advanced Research Projects Agency, Department of Defense, ARPA Order #1092 and SAMSO, AFSC, Deputy for Re-entry Systems (SMY), Norton Air Force Base, Cal. 92409.

13 ABSTRACT

Radiation profiles in an ablating flat plate Air-Teflon laminar boundary layer have been studied both experimentally and theoretically. The experiments were conducted in a one atmosphere, 3000 - 6000°K, subsonic free stream produced by an arc jet. Spatially resolved radiation profiles within the boundary layer were obtained in both the visible and near infrared. Spatially integrated boundary layer radiation was measured in the 4 - 10μ region. The major radiation in the visible and near ultraviolet wavelengths was the CN violet. In the infrared, the major radiators were CO, CO_2, NO and COF_2. The theory which was developed to predict the structure included coupling of the heat and mass transfer at the Teflon surface. A "partial equilibrium" model for the Teflon-Air chemistry was utilized, which does not allow the formation of CF_3 and CF_4 within the boundary layer. For the selected wavelengths in the infrared the theory generally predicted quite well both the spatial location and magnitude of the peak radiation, and also predicted the integrated radiation across the layer to within a factor of two. For the selected wavelength in the visible, the radiation intensity, which comes from CN, is much larger than predicted, indicating that the CN is not in thermodynamic equilibrium.

DD FORM 1 JAN 64 1473

UNCLASSIFIED

Security Classification

14 KEY WORDS	LINK A		LINK B		LINK C	
	ROLE	WT	ROLE	WT	ROLE	WT
1. Boundary Layer 2. Ablation 3. Teflon Ablation 4. Infrared Spectra 5. CO Radiation 6. CO_2 Radiation 7. COF_2 Radiation						

INSTRUCTIONS

1. ORIGINATING ACTIVITY: Enter the name and address of the contractor, subcontractor, grantee, Department of Defense activity or other organization *(corporate author)* issuing the report.

2a. REPORT SECURITY CLASSIFICATION: Enter the overall security classification of the report. Indicate whether "Restricted Data" is included. Marking is to be in accordance with appropriate security regulations.

2b. GROUP: Automatic downgrading is specified in DoD Directive 5200.10 and Armed Forces Industrial Manual. Enter the group number. Also, when applicable, show that optional markings have been used for Group 3 and Group 4 as authorized.

3. REPORT TITLE: Enter the complete report title in all capital letters. Titles in all cases should be unclassified. If a meaningful title cannot be selected without classification, show title classification in all capitals in parenthesis immediately following the title.

4. DESCRIPTIVE NOTES: If appropriate, enter the type of report, e.g., interim, progress, summary, annual, or final. Give the inclusive dates when a specific reporting period is covered.

5. AUTHOR(S): Enter the name(s) of author(s) as shown on or in the report. Enter last name, first name, middle initial. If military, show rank and branch of service. The name of the principal author is an absolute minimum requirement.

6. REPORT DATE: Enter the date of the report as day, month, year, or month, year. If more than one date appears on the report, use date of publication.

7a. TOTAL NUMBER OF PAGES: The total page count should follow normal pagination procedures, i.e., enter the number of pages containing information.

7b. NUMBER OF REFERENCES: Enter the total number of references cited in the report.

8a. CONTRACT OR GRANT NUMBER: If appropriate, enter the applicable number of the contract or grant under which the report was written.

8b, 8c, & 8d. PROJECT NUMBER: Enter the appropriate military department identification, such as project number, subproject number, system numbers, task number, etc.

9a. ORIGINATOR'S REPORT NUMBER(S): Enter the official report number by which the document will be identified and controlled by the originating activity. This number must be unique to this report.

9b. OTHER REPORT NUMBER(S): If the report has been assigned any other report numbers *(either by the originator or by the sponsor)*, also enter this number(s).

10. AVAILABILITY/LIMITATION NOTICES: Enter any limitations on further dissemination of the report, other than those imposed by security classification, using standard statements such as:

(1) "Qualified requesters may obtain copies of this report from DDC."

(2) "Foreign announcement and dissemination of this report by DDC is not authorized."

(3) "U. S. Government agencies may obtain copies of this report directly from DDC. Other qualified DDC users shall request through

_____."

(4) "U. S. military agencies may obtain copies of this report directly from DDC. Other qualified users shall request through

_____."

(5) "All distribution of this report is controlled. Qualified DDC users shall request through

_____."

If the report has been furnished to the Office of Technical Services, Department of Commerce, for sale to the public, indicate this fact and enter the price, if known.

11. SUPPLEMENTARY NOTES: Use for additional explanatory notes.

12. SPONSORING MILITARY ACTIVITY: Enter the name of the departmental project office or laboratory sponsoring *(paying for)* the research and development. Include address.

13. ABSTRACT: Enter an abstract giving a brief and factual summary of the document indicative of the report, even though it may also appear elsewhere in the body of the technical report. If additional space is required, a continuation sheet shall be attached.

It is highly desirable that the abstract of classified reports be unclassified. Each paragraph of the abstract shall end with an indication of the military security classification of the information in the paragraph, represented as *(TS), (S), (C), or (U)*

There is no limitation on the length of the abstract. However, the suggested length is from 150 to 225 words.

14. KEY WORDS: Key words are technically meaningful terms or short phrases that characterize a report and may be used as index entries for cataloging the report. Key words must be selected so that no security classification is required. Identifiers, such as equipment model designation, trade name, military project code name, geographic location, may be used as key words but will be followed by an indication of technical context. The assignment of links, rules, and weights is optional